catalysts

MDPI

Article

Preparation and Properties of g-C_3N_4-TiO_2 Cement-Based Materials Supported by Recycled Concrete Powder

Teng Yuan [1] and Wu Yao [1,2,*]

[1] School of Materials Science and Engineering, Tongji University, Shanghai 201804, China
[2] Key Laboratory of Advanced Civil Engineering Materials of Ministry of Education, School of Materials Science and Engineering, Tongji University, Shanghai 201804, China
* Correspondence: yaowuk@tongji.edu.cn

Abstract: In this paper, recycled concrete powder (RCP) is used as the carrier of g-C_3N_4-TiO_2 instead of natural minerals. The prepared g-C_3N_4-TiO_2/RCP composites were characterized by X-ray diffractometer, scanning electron microscope, infrared spectrometer, specific surface area analyzer, UV-visible spectrophotometer, and RhB solution degradation experiments. The results show that the rough, porous structure of RCP was beneficial to the stable load of g-C_3N_4-TiO_2. Under the condition that the content of g-C_3N_4-TiO_2 catalyst is constant, the agglomeration of g-C_3N_4-TiO_2 can be reduced by using RCP as a carrier, thus improving its photocatalytic efficiency. Subsequently, g-C_3N_4-TiO_2/RCP was loaded onto the surface of cement-based materials by coating bonding method to study its photocatalytic performance. It is found that the photocatalytic cement-based material has a similar degradation effect on the degradation of surface RhB as g-C_3N_4-TiO_2/RCP in RhB solution. Our work may open up a new field for the recycling of RCP and provide new ideas for the development of photocatalytic cement-based materials.

Keywords: recycled concrete powder; g-C_3N_4-TiO_2; photocatalytic cement-based materials

Citation: Yuan, T.; Yao, W. Preparation and Properties of g-C_3N_4-TiO_2 Cement-Based Materials Supported by Recycled Concrete Powder. *Catalysts* **2023**, *13*, 312. https://doi.org/10.3390/catal13020312

Academic Editors: Zhengxian Yang, Lu Yang and Manuel Filipe P. C. M. Costa

Received: 14 January 2023
Revised: 28 January 2023
Accepted: 29 January 2023
Published: 31 January 2023

1. Introduction

The rapid development of industrialization has led to more and more serious pollution and environmental deterioration, and has begun to pose a threat to human health. The treatment of water pollutants has achieved good results, but it also faces more new challenges [1,2]. In order to implement the concept of 'sustainable development' and effectively control environmental pollution, photocatalytic technology has begun to attract more researchers' attention [3]. Cement-based composite material is one of the most vital civil engineering materials, which is widely used in the field of building materials. Some researchers have proposed combining photocatalytic technology with building materials [4]. Loading photocatalyst on cement-based materials to prepare photocatalytic cement-based materials can degrade pollutants on the cement surface to protect cement-based materials from being destroyed by pollutants [4–6]. Early researchers chose to combine Nano-TiO_2 with cement to prepare photocatalytic cement-based materials. Nano-TiO_2 is a mature photocatalytic material which has the advantages of stable physical and chemical properties, non-toxic, low cost, and excellent photocatalytic activity under ultraviolet light [3,7,8]. However, Nano-TiO_2 is a photocatalyst that is easily agglomerated, which makes it impossible to fully expose the active sites in use [9,10]. Therefore, how to disperse TiO_2 has become a research hotspot [11]. At the same time, Nano-TiO_2 has a poor response under visible light, and the proportion of visible light in natural light is much larger than that of ultraviolet light, which limits the development of photocatalytic cement-based materials in natural light scenarios [12,13]. The semiconductor composite method is a very common and effective way of semiconductor modification [14–16]. In order to prepare photocatalysts with enhanced visible light catalytic ability, z-type g-C_3N_4-TiO_2 heterojunction photocatalysts were prepared [12,17,18]. Compared with ordinary TiO_2 and g-C_3N_4,

the g-C_3N_4-TiO_2 photocatalyst exhibits higher photocatalytic activity under visible light irradiation. This is because the z-scheme heterojunction between g-C_3N_4 and TiO_2 allows for efficient separation of the photogenic electrons and holes (h^+/e^-), thereby improving the photocatalytic ability [17,19,20]. At the same time, g-C_3N_4-TiO_2 has comprehensive degradation performance, which can degrade organic dyes (such as MB solution, RhB solution, etc.) and gas pollutants (such as N_2O, etc.) [21,22].

In recent years, nano photocatalyst dispersed and fixed on the surface of porous materials has become a new research highlight, providing more active sites for photocatalytic reactions and also improving the concentration of pollutants near the active sites by means of the adsorption capacity of porous carrier materials, as it accelerates the photocatalytic reaction rate and synergistically enhances the ability of photocatalyst to degrade pollution [9,23,24]. Currently, the main supporting materials for nano-TiO_2 are natural minerals such as zeolite [9,11,23,25]. Zeolite is a widely used carrier at present. It has good adsorption performance and porous structure, which is conducive to the adhesion of catalyst. However, its high cost limits its development [23]. The fine dust (also known as recycled concrete powder) produced during the crushing process of concrete waste has not been fully reused [26–28]. In order to promote the reuse of RCP resources, people have begun to explore RCP as supplementary cementitious materials and so on. However, in fact, the recycled powder recycling scene is still very limited [29,30].

However, RCP is mainly composed of hydration products of cement [31]. RCP has strong inertness after hydration and carbonization, and the surface forms a rough porous structure, which is suitable for supporting photocatalysts, because the support material needs to provide sufficient surface space to accommodate photocatalysts while maintaining the stability of physical and chemical properties in photocatalytic reactions [10,11,32,33]. At the same time, some components of RCP such as quartz and calcium carbonate have been successfully used as photocatalyst TiO_2 carriers in practice [34]. Inspired by this, it is theoretically feasible to use RCP as the carrier of photocatalyst. In addition, from the perspective of solid waste recycling, the use of RCP as a carrier to prepare composite photocatalysts is cost-effective [30,35]. At the same time, the early loading method (surface coating method, internal mixing method, etc.) has poor durability, and the stabilizer is easy to wear off from the surface of cement-based materials, which brings limitations to the development of photocatalytic cement-based materials [4,14,36–38].

At present, most of the carriers used to load catalysts will bring higher costs, and most of the modified catalysts with TiO_2 series have a poor response to light. In order to reuse RCP and improve the utilization rate of natural light resources and the durability of photocatalytic cement-based materials. In this study, RCP was used as a carrier to support g-C_3N_4-TiO_2 composites that can effectively reduce the agglomeration of g-C_3N_4-TiO_2, which has an excellent visible light response [39]. The g-C_3N_4-TiO_2/RCP composites were prepared by mechanochemical method [34,39,40]. The photocatalytic degradation of RhB under visible light was carried out to evaluate the photocatalytic performance of the prepared g-C_3N_4-TiO_2/RCP composites. The binding mechanism of g-C_3N_4-TiO_2/RCP composites was studied in detail. The role of RCP in the process of affecting the band structure and photocatalytic performance of g-C_3N_4-TiO_2 was studied. Finally, g-C_3N_4-TiO_2/RCP was prepared into coating by using potassium silicate as adhesive and loaded on cement-based materials. After g-C_3N_4-TiO_2/RCP was successfully loaded onto the cement surface, the surface pollutants were degraded under visible light to evaluate the photocatalytic performance of g-C_3N_4-TiO_2/RCP photocatalytic cement-based materials. As a cost-effective and stable carrier, RCP may be widely used in the field of photocatalytic cement-based materials in the future. Our work may open up a new field for the recycling of RCP and provide new ideas for the development of photocatalytic cement-based materials.

2. Results and Discussion

2.1. Microstructure of RCP and g-C_3N_4-TiO_2/RCP Composites

Figure 1a describes the microstructure of RCP. The rough and porous surface structure can be observed, which can provide a large number of loading sites for g-C_3N_4-TiO_2 [11]. As can be seen from the particle size distribution curve in Figure 1b, the median particle size d_{50} of RCP is about 7 μm and the particle size range is about 3~150 μm. The particle size of RCP is beneficial to the combination of RCP and g-C_3N_4-TiO_2 in nano-micro size. Figure 1c is the morphology of g-C_3N_4-TiO_2. It can be observed that its shape is flocculated, and the surface has a granular feeling.

The microstructure of g-C_3N_4-TiO_2/RCP composites is shown in Figure 2a. The surface of gT(20%)R is flocculent, and g-C_3N_4-TiO_2 are densely distributed on the surface of RCP, as shown by arrows. The EDS results of Spot confirm that these flocculent substances are g-C_3N_4-TiO_2, which proves that g-C_3N_4-TiO_2 is successfully loaded on RCP. The element mapping of gT(20%)R is shown in Figure 2b–f. It can be clearly seen that the Ti, O, and N elements are uniformly distributed in the field of view and the imprinting overlap each other, indicating that the g-C_3N_4-TiO_2 is uniformly distributed on the surface of RCP [30]. This may be due to the fact that RCP is a good carrier for g-C_3N_4-TiO_2 and has a certain fixing effect on g-C_3N_4-TiO_2 [11].

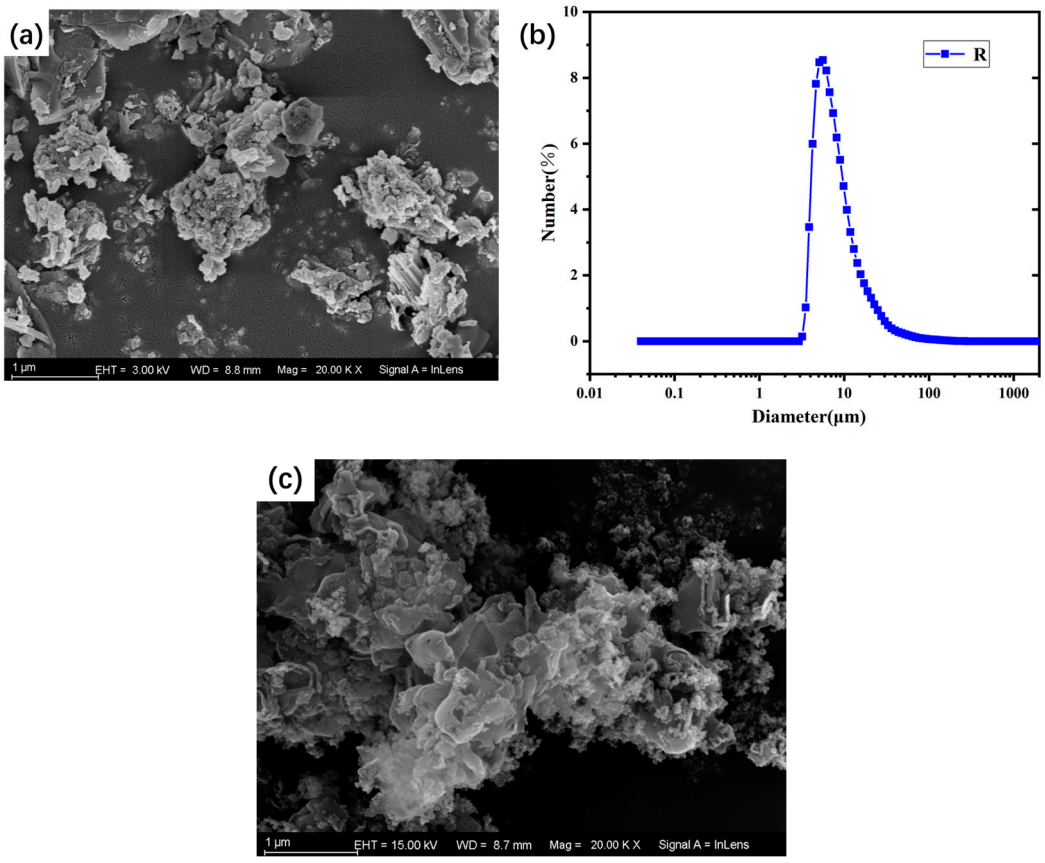

Figure 1. (**a**) Micro-morphology of RCP; (**b**) particle size distribution curve of RCP; (**c**) SEM image of gT.

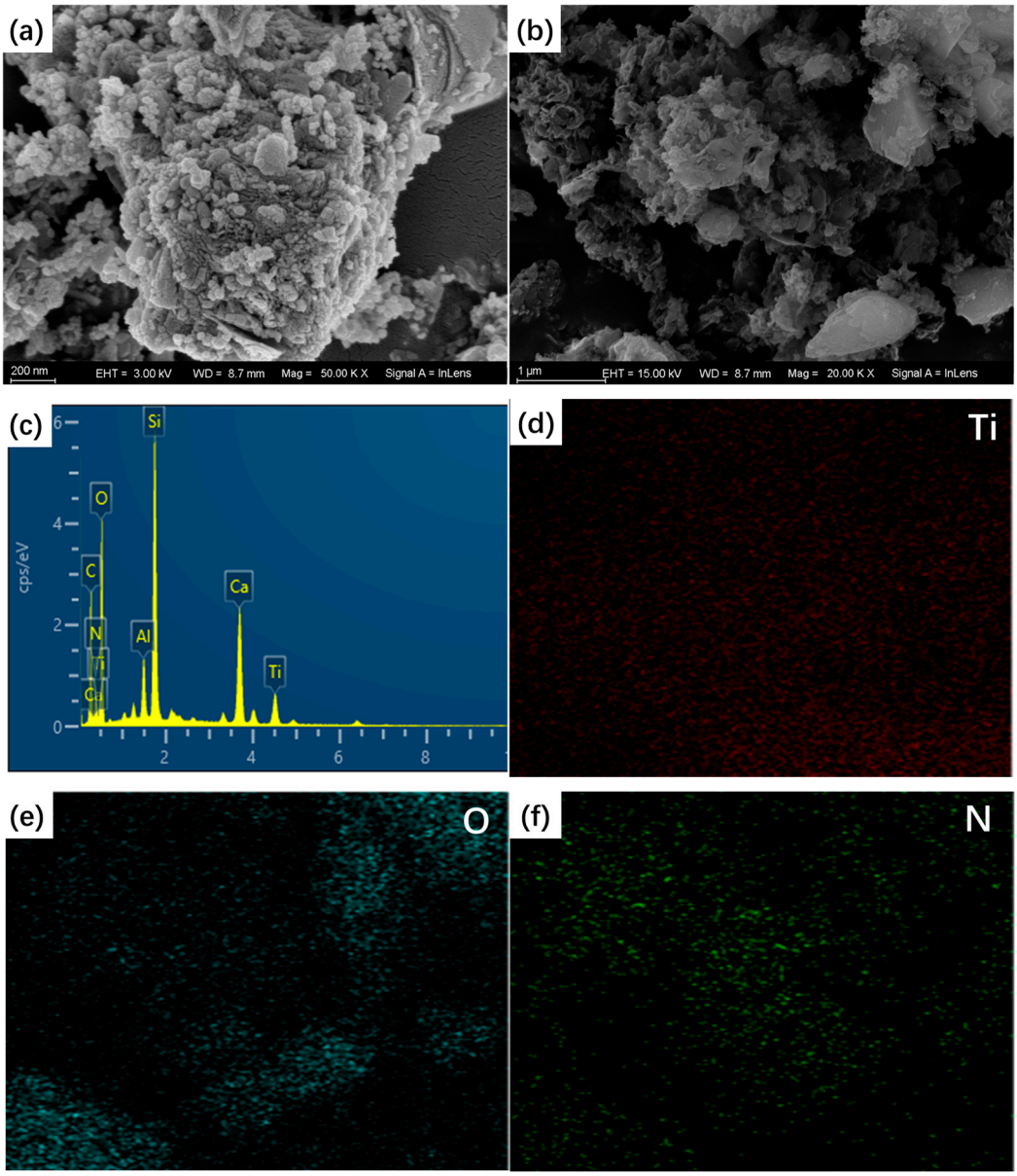

Figure 2. (**a**–**f**) SEM images and elements distribution of gT(20%)R.

2.2. Crystal Phase of RCP and g-C_3N_4-TiO_2/RCP Composites

As shown in Figure 3a, the main crystalline phases of RCP are calcite and quartz, which are carbonized products and cement paste, respectively. In the hydration products of cement, amorphous calcium silicate hydrate (C-S-H) cannot be detected by X-ray diffraction [30]. Figure 3b presents the phase composition of g-C_3N_4-TiO_2/RCP. The g-C_3N_4 has two obvious peaks at 2θ, which are 13.1° and 27.4°, which are the typical diffraction peaks (100) and (002) of g-C_3N_4, respectively [12]. The (100) crystal plane is inter-planar stacking, and the (002) crystal plane is interlayer stacking of aromatic segments [13]. TiO_2 is composed of anatase and rutile TiO_2. The (110) peak of rutile TiO_2 at 27.4° overlaps with the (002) peak of g-C_3N_4 [3]. XRD analysis showed that g-C_3N_4 and TiO_2 were combined in g-C_3N_4-TiO_2. The main peak shape of g-C_3N_4-TiO_2/RCP is basically the same as that of RCP, which may be due to the fact that g-C_3N_4-TiO_2 is attached to the holes of RCP. When the proportion of g-C_3N_4-TiO_2 exceeds 20%, some peak shapes of g-C_3N_4-TiO_2 will be highlighted.

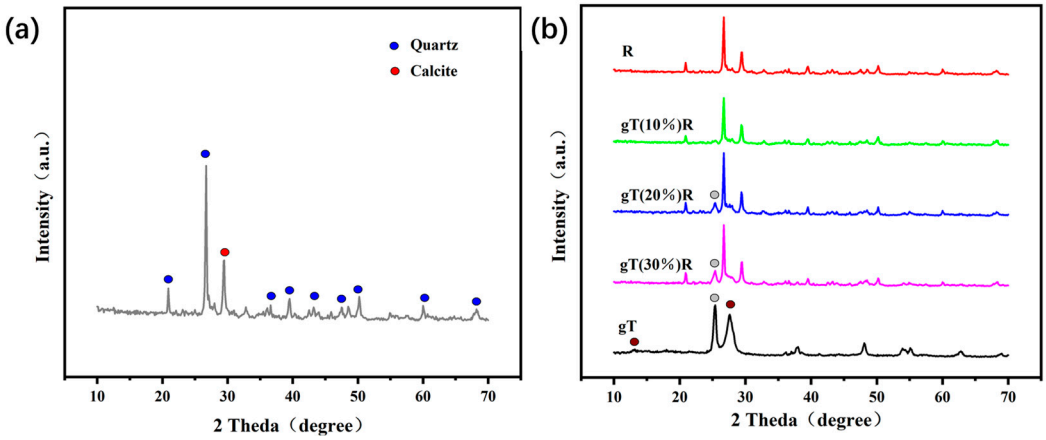

Figure 3. X-ray diffraction patterns of (**a**) RCP and (**b**) g-C_3N_4-TiO_2/RCP composites.

2.3. Surface Area and Pore Structure g-C_3N_4-TiO_2/RCP Composites

As shown in Figure 4a, the N_2 adsorption–desorption isotherms of the samples are a mixture of type III and type V according to IUPAC classification. At higher relative pressure, a small hysteresis loop can be observed in the sample, and the adsorption amount of N_2 increases sharply, indicating the presence of a mesoporous structure in the sample [34]. After loading g-C_3N_4-TiO_2, the N_2 adsorption capacity of gT(20%)R increased significantly due to the increase of specific surface area (SSA). As shown in Figure 4b, the pore content of gT(20%)R (pore size greater than 30 nm) is lower than that of RCP, which may indicate that g-C_3N_4-TiO_2 is loaded in the macropores of RCP and occupies the pore space on RCP. The pore content of gT(20%)R is higher than that of RCP (pore diameter is less than 30 nm), which indicates that a large number of micropores of g-C_3N_4-TiO_2 and RCP in gT(20%)R still exist, which ensures the ability of adsorption and degradation of gT(20%)R. The larger specific surface area can provide more surface-active sites, thereby enhancing photocatalysis. While ensuring a certain photocatalytic efficiency, the less the amount of g-C_3N_4-TiO_2, the higher the cost performance and efficiency of its practical application. The SSA of gT(20%)R increased to 27.4046 m^2/g after loading g-C_3N_4-TiO_2. The results show that the rough surface and porous structure of RCP are beneficial to the loading and dispersion ofg-C_3N_4-TiO_2.

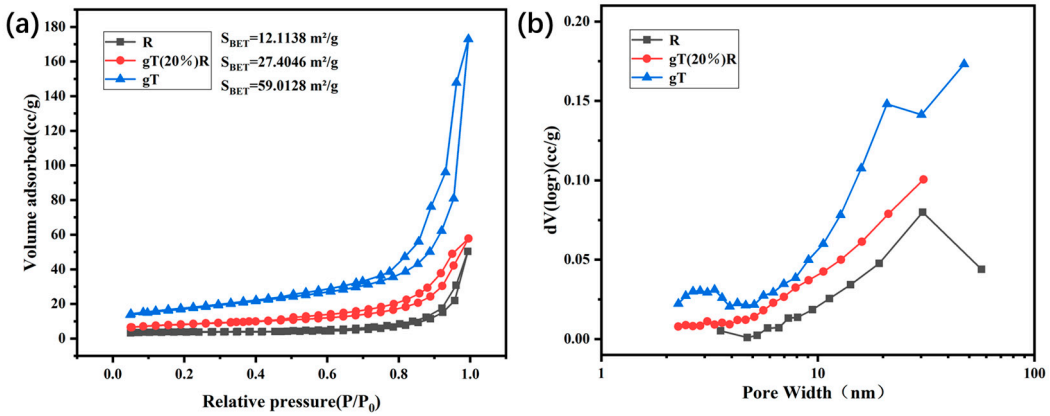

Figure 4. (**a**) N_2 adsorption–desorption isotherms; (**b**) pore size distribution curves.

2.4. Binding Mechanism between RCP and g-C_3N_4-TiO_2

Figure 5 shows the FT-IR spectra of alkali-treated RCP. The absorption peak at 1084 cm^{-1} is caused by the antisymmetric stretching vibration of the Si-O-Si bond [41]. Compared with RCP, the intensity of the absorption peak of gT(x)R (x = 10%, 20%, 30%)

decreased significantly. In addition to the decrease of RCP content, it may also be that the interaction between g-C_3N_4-TiO_2 and RCP leads to the fracture of some Si-O-Si bonds. The absorption peak intensity of CO_3^{2-} at 1447 cm^{-1} decreases with the increase of g-C_3N_4-TiO_2 content, which may be due to the partial destruction of CO_3^{2-} during the loading of g-C_3N_4-TiO_2 on RCP [42]. The absorption peak in the range of 3250~3750 cm^{-1} is generally regarded as a symbol of hydroxyl group. Compared with gT and RCP, the intensity of gT(x)R (x = 10%, 20%, 30%) absorption peaks are enhanced to varying degrees. This may be due to the change of the surface chemical environment of gT(x)R (x = 10%, 20%, 30%) ball milled in ethanol medium for 4 h, and the number of hydroxyl groups on the surface of gT(x)R (x = 10%, 20%, 30%) increased.

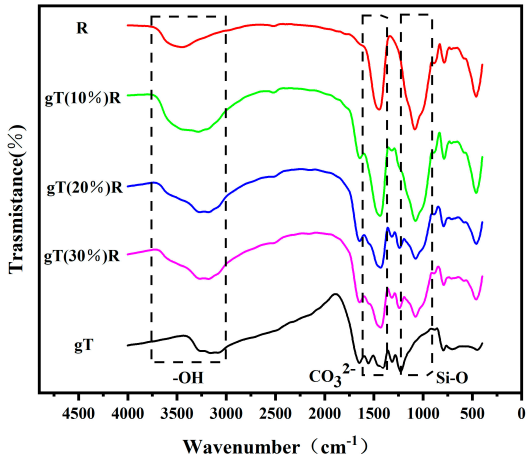

Figure 5. Fourier-transform infrared (FT-IR) spectra of gT(x)R (x = 0, 10%, 20%, 30%, 100%).

2.5. Photocatalytic Performance of g-C_3N_4-TiO_2/RCP Composites

Figure 6a compares the photocatalytic performance of different samples. In the dark treatment, the concentration of RhB decreases slightly, which is due to the adsorption of RhB by g-C_3N_4-TiO_2/RCP composite. When the visible light was turned on, the concentration of RhB decreased with the extension of irradiation time, but the rate of decline was different for different samples. Photocatalytic efficiency is gT(30%)R, gT(20%)R, gT(20%)R in descending order. This can be simply explained as the photocatalytic efficiency increasing with the increase of g-C_3N_4-TiO_2 content in g-C_3N_4-TiO_2/RCP. In the actual situation, when the content of g-C_3N_4-TiO_2 increases from 10% to 20%, the photocatalytic efficiency is significantly improved. However, when the content of g-C_3N_4-TiO_2 increases from 20% to 30%, the increase range of photocatalytic efficiency seriously decreases. This is because the photocatalytic efficiency depends on the number of active sites, and g-C_3N_4-TiO_2 is easy to agglomerate. As a carrier, RCP can effectively disperse g-C_3N_4-TiO_2, reduce the agglomeration effect, and increase the active site. The catalyst content of gT(30%)R is the same as that of gT samples, but the photocatalytic efficiency is gT(30%)R > gT, which also proves that RCP can improve the agglomeration of g-C_3N_4-TiO_2. As shown in Figure 6b, when the content of g-C_3N_4-TiO_2 increases from 10% to 20%, the k_{app} of g-C_3N_4-TiO_2/RCP composites increases from 0.02698 min^{-1} to 0.05168 min^{-1}, an increase of 91.55%. However, when the content of g-C_3N_4-TiO_2 increases from 20% to 30%, k_{app} increases from 0.05168 min^{-1} to 0.06127 min^{-1}, an increase of 18.56%, and the growth range obviously decreases. At the same time, the reaction rate is gT(30%)R (0.06127 min^{-1}) > gT (0.05287 min^{-1}), and the content of g-C_3N_4-TiO_2 in these two samples is the same, which is also consistent with the above conclusion. RCP as a carrier can effectively disperse g-C_3N_4-TiO_2, reduce the agglomeration effect, and increase the active site.

Figure 6c shows the cyclic photocatalytic performance of gT(20%)R. It can be observed that the photocatalytic performance of gT(20%)R is stable. After three cycles of degradation tests, the degradation rate and degradation rate change little. The stable photocatalytic

performance fully proves that g-C_3N_4-TiO_2 is firmly combined with RCP, which effectively avoids the loss of g-C_3N_4-TiO_2 in the cycle degradation process.

Figure 6d provides the x-ray images before and after the gT(20%)R cyclic degradation experiment. It can be observed that the phase composition of gT(20%)R did not change, and only the intensity of some characteristic peaks of g-C_3N_4-TiO_2 decreased. This may be due to the occupation of the active reaction sites and the loss of g-C_3N_4-TiO_2 [34]. The stable photocatalytic performance indicates that g-C_3N_4-TiO_2 is closely combined with RCP and can reduce the loss of g-C_3N_4-TiO_2 during the cycle.

Figure 6e is the scanning spectrum of RhB solution in the wavelength range of 450–650 nm during the degradation of RhB solution by gT(20%)R. It can be observed that the maximum absorption wavelength of the solution is always at 554 nm, which is consistent with the conclusion of the literature [43].

In conclusion, RCP can not only reduce the consumption of g-C_3N_4-TiO_2, but also alleviate the agglomeration effect of g-C_3N_4-TiO_2, thus improving the photocatalytic efficiency of pure g-C_3N_4-TiO_2. As a functionalized carrier of g-C_3N_4-TiO_2 nanoparticles, RCP significantly improves the added value of itself.

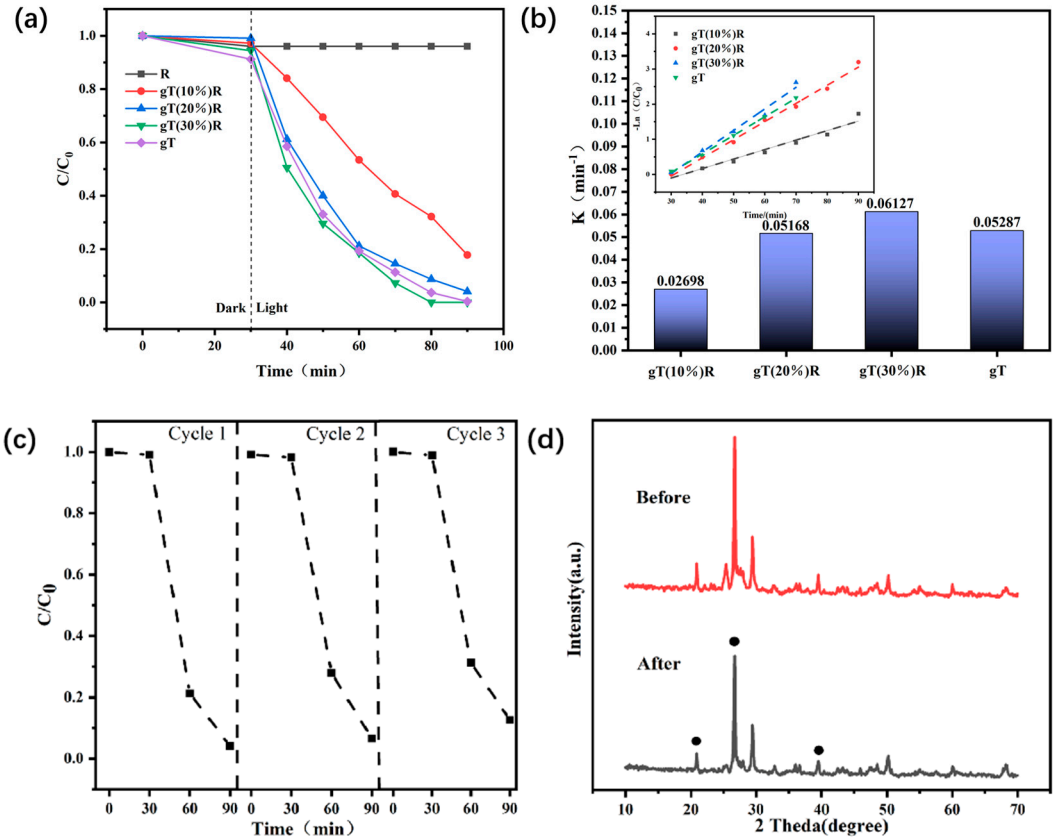

Figure 6. *Cont.*

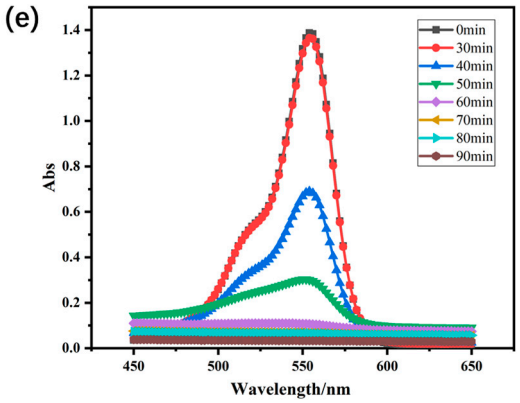

Figure 6. (**a**) Photocatalytic degradation efficiency; (**b**) Linear fitting of -Ln C/C_0 and time, and corresponding apparent rate constant; (**c**) Cyclic degradation experiment of gT(20%)R; (**d**) X-ray patterns of gT(20%)R before and after cyclic degradation experiment; (**e**) Scanning spectrum of the solution in the wavelength range of 450–650 nm during the degradation of RhB solution by gT(20%)R.

2.6. Band Gap and Absorption Edge of g-C_3N_4-TiO_2/RCP Composites

The photocatalytic efficiency of semiconductors is related to the separation and transfer ability of charge carriers, and the band structure of g-C_3N_4-TiO_2 determines the photocatalytic efficiency of semiconductors. Figure 7a shows the UV-Vis diffuse reflectance spectra of R, gT(10%)R, gT(20%)R, gT(30%)R, and gT. The inset of Figure 7a is a partially enlarged picture (350–450 nm). The absorbance of RCP does not exhibit the typical absorbance of semiconductors. For sample gT, the absorbance began to decline sharply when the wavelength reached 400 nm, which was due to the heterojunction effect between g-C_3N_4 and TiO_2, which widened the absorption range of TiO_2, namely, the visible light response field [20]. Meanwhile, for other samples, it shows that these samples can absorb visible light by generating hole electron pairs.

However, the absorption edge of gT(x)R (x = 20%, 30%) has a blue shift relative to gT. By Tauc mapping [44], the band gap energy of gT(20%)R (2.91 eV) is higher than that of gT (2.95 eV), as shown in Figure 7b. This may be due to the quantum range effect when gT is in a highly discrete state. The wider band gap of gT(20%)R makes it easier to suppress hole–electron recombination and increase carrier lifetime. The absorption edge of gT(20%)R shifted slightly towards the visible light direction. This may indicate that the band structure of g-C_3N_4-TiO_2 changed after interacting with RCP. The interaction mechanism between RCP and g-C_3N_4-TiO_2 is shown in Figure 7c. After mechanical ball milling, a large number of unsaturated sites are generated on the surface of RCP and interact with g-C_3N_4-TiO_2. The surface polarization of g-C_3N_4-TiO_2 was induced. Under this polarization effect, electrons tend to transfer from g-C_3N_4-TiO_2 to RCP [34].

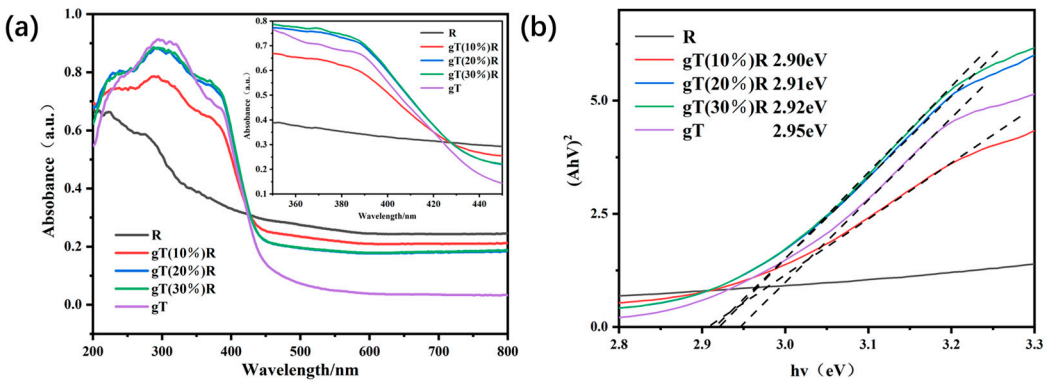

Figure 7. *Cont.*

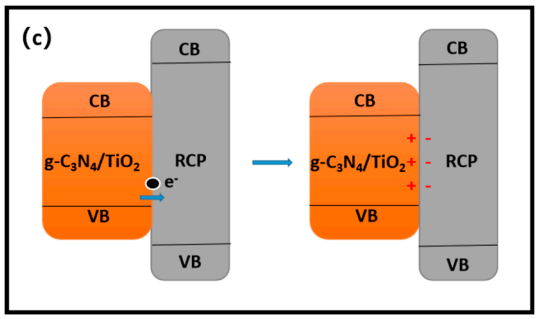

Figure 7. (**a**) UV-VIS diffusive reflectance spectra of RCP, gT(10%)R, gT(20%)R, gT(30%)R, and gT; (**b**) Plots of $(Ah\nu)^2$ vs. hν; (**c**) The mechanism of the interaction between g-C_3N_4-TiO_2 and RCP.

2.7. Performance Evaluation of Photocatalytic Cement

The mechanism of coating bonding method, potassium silicate, reacts with the surface of incompletely carbonized cement blocks to form a more stable bond, and g-C_3N_4-TiO_2/RCP is stably loaded on the surface of cement-based materials [14].

Self-cleaning ability is one of the significant characteristics of photocatalytic cement-based materials. Under the action of light, the surface beauty of cement-based materials can be continuously maintained. Figure 8 shows the removal effect of RhB by photocatalytic cement-based materials prepared by coating bonding method under visible light conditions. As shown in Figure 8, comparing the photos before and after the photocatalytic experiment under visible light irradiation, it was found that with the increase of illumination time, the color of the surface of the regenerated differential load cement basically did not change, while the color of the samples loaded with gT(x)R became lighter to varying degrees. This shows that the cement has a self-cleaning function after loading gT(x)R. This is because the catalyst on the cement surface degrades part of the dye. However, the self-cleaning efficiency of different samples is different. In terms of color contrast, after 60 min of illumination, the fading of gT(30%) R group was the most obvious, followed by gT(20%)R, and the fading degree of gT(10%) R was not obvious, which was consistent with the rule of gT(x)R degrading RhB in liquid. This shows that the performance of the catalyst has not changed after loading gT(x)R to the cement surface by coating bonding method.

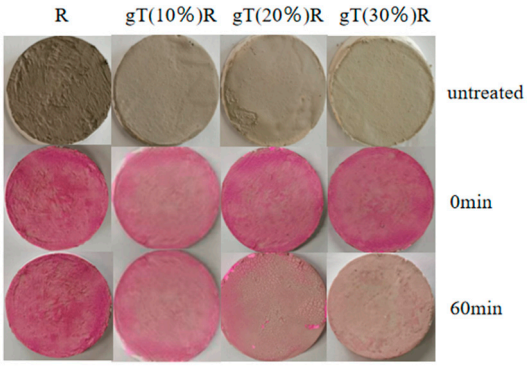

Figure 8. The apparent figures before and after degradation of RhB dye by cement-based materials loaded with gT(x)R (x = 0, 10%, 20%, 30%).

3. Materials and Methods

3.1. Raw Materials

The urea, melamine, and analytically pure Rhodamine B (RhB) were purchased from Sinopharm Chemical Reagent Co., Ltd. (Shanghai, China). Potassium silicate was purchased from Henan Jinrun New Materials Co., Ltd. (Gongyi, China). White cement was purchased from Anhui Conch Cement Co. Ltd. (Wuhu, China). The nano-TiO_2 was purchased from Shanghai Titan Technology Co., Ltd. (Shanghai, China). RCP was provided by

Shanghai Youhong Environmental Protection Technology Co., Ltd. (Shanghai, China). The chemical composition of RCP is shown in Table 1.

Table 1. Chemical composition of RCP (wt%).

SiO_2	CaO	Al_2O_3	Fe_2O_3	MgO	K_2O	Na_2O	SO_3	TiO_2	MnO
47.49	31.03	11.71	2.96	2.04	1.85	1.08	0.92	0.56	0.36

3.2. Preparation of g-C_3N_4-TiO_2 Composites

The preparation process of g-C_3N_4-TiO_2 is shown in Figure 1. First, urea and melamine were mixed at a mass ratio of 3:1, then ethanol was added and ground thoroughly. After the ethanol was completely volatilized, the mixture was wrapped in tin foil and placed in an alumina crucible with a lid. The mixture was then calcined in a muffle furnace at a heating rate of 5 °C/min to 550 °C for 120 min. Finally, the product was ground into powder to obtain g-C_3N_4. The newly prepared g-C_3N_4 and TiO_2 nanoparticles were loaded in a 25 mL round-bottom flask with a mass ratio of 3:1, and ethanol was added as the solvent. The solution was ultrasonic treated in bath ultrasound for 1 h (model: wu-d22h; Dahan Technology Co., LTD, Jinan, China), and the ultrasonic frequency and power are 20 kHz and 100 w, respectively. The treated solution was placed in an oven at 80 °C to dry, and the dried sample was ground into powder to prepare g-C_3N_4-TiO_2 nanocomposites.

3.3. Preparation of g-C_3N_4-TiO_2/RCP Composites

The g-C_3N_4-TiO_2/RCP composites were prepared by mechanical ball milling. RCP used in this study was collected from the fine powder of waste concrete after crushing. First, a certain amount of RCP was stirred with deionized water for 20 min to obtain RCP slurry. At the same time, g-C_3N_4-TiO_2 and deionized water were ultrasonically treated for 1 h to obtain the suspension of g-C_3N_4-TiO_2. Subsequently, the uniformly dispersed suspension of g-C_3N_4-TiO_2 was mixed with RCP slurry, and then stirred until uniform. The mass ratio of solid powder to water in the mixture was 30%. The mixture was then poured into a 200 mL agate jar with a mass ratio of agate balls to solid powder of 4:1. We ground the mixed slurry with a planetary ball mill (QM-3 SP 2, Nanjing Nanda Instrument Factory) at a speed of 1000 rpm. Finally, the slurry mixture was dried at 110 °C for 24 h, and the product was ground to obtain g-C_3N_4-TiO_2/RCP composite material. The g-C_3N_4-TiO_2/RCP samples are labeled as gT(x)R, where x represents the content proportion of g-C_3N_4-TiO_2, (x = 10%, 20%, 30%). The pure g-C_3N_4-TiO_2 powder is named gT, and the pure RCP powder is abbreviated as R.

3.4. Characterization of g-C_3N_4-TiO_2/RCP

Scanning electron microscope (SEM) (TM4000 Plus, Hitachi, Tokyo, Japan) was used to observe the microstructure of the material surface, and energy dispersive spectrometer (Model 550 I, IXRF Systems, Austin, TX, USA) was used to analyze the distribution of elements in the microscopic area of the material. X-ray diffraction (d/max 2550, Rigaku, Tokyo, Japan) was used to analyze the phase of the material. The copper Ka-ray source worked at 40 kV and 100 mA. Ultraviolet-visible diffuse reflectance spectroscopy (DRS) was measured on a spectrophotometer (U-4100, Hitachi, Tokyo, Japan) with an integrating sphere, and the scanning range is 800–200 cm^{-1}. The BET specific surface area and pore size distribution were measured by BET automatic specific surface area and porosity analyzer (ASAP2460, Micromeritics, Norcross, GA, USA). Fourier transform infrared (FT-IR) spectroscopy was recorded by an infrared spectrometer (Equinox 55, Bruker, Heidelberg, Germany) with a scanning range of 4000–400 cm^{-1}.

3.5. Surface Treatment of Cement with g-C_3N_4-TiO_2/RCP

For the preparation of cement samples, weigh white cement and water with appropriate quality according to the water–cement ratio of 0.4, then add them into the paste mixer

to stir for 3 min. Transfer the stirred slurry to a round mold with a diameter of 50 mm and a height of 5 mm, put it on a shaking table for 1 min, then scrape off the surface, cover it with plastic wrap, and put it into a curing box. The temperature of the curing box was set to 20 °C and the humidity was 90%. After 1 day of curing, the sample was demolded and placed in the curing box for 7 days. After 1 day of curing, the sample was demolded and placed in the curing box for 7 days. R, gT(10%)R, gT(20%)R, and gT(30%)R were selected as the required photocatalyst samples. Each sample was taken 1 g, and 1 g potassium silicate solution and 1 g water were added respectively for sufficient mechanical stirring. When the mixture is uniform and has a certain fluidity, it proves that the coating has been successfully prepared. The catalyst was supported on the surface of cement matrix by coating bonding method. The loading steps are as follows: the dispersion is evenly applied to the cement surface by a brush, and the treatment is completed after repeating three times from left to right. After the treated cement samples were stored in a dark box (temperature: 20 °C) for 7 days, the cement surface was completely dry, which indicates that the photocatalytic cement is successfully prepared.

3.6. Assessment of Photocatalytic Performance

The photocatalytic performance of g-C_3N_4-TiO_2/RCP composites was evaluated by visible light degradation. The light source is a 150W visible light lamp (wavelength range 400~780 nm). The experimental process is as follows.

Firstly, the five samples were subjected to degradation tests in order, 200 mg of R, gT (10%)R, gT(20%)R, gT(30%)R and 60 mg of g-C_3N_4-TiO_2 were added to 50 mL of RhB solution (7.5 mg/L) and mixed in dark for 30 min to reach adsorption equilibrium. Then, the visible light was turned on, and 2.5 mL of RhB solution was sampled every 10 min. Finally, the collected RhB solution was centrifuged at 7000 rpm in a high-speed centrifuge for 5 min. The absorbance of the centrifuged RhB solution was measured by UV-Vis spectrophotometer (UV 1800, Jinghua, China) in the scanning range of 800–200 cm^{-1}. Rinsed gT(20%)R 5 times with deionized water and dried in an 80 °C oven for cyclic degradation tests. The concentration of RhB was calculated by the absorbance at the maximum absorption wavelength (554 nm) of RhB according to Beer-Lambert Law. C/C_0 is used to represent the photocatalytic efficiency (C_0 is the initial concentration of RhB, and C is the concentration of RhB at time t). The kinetic parameters of photocatalytic reaction in photocatalytic stage were studied by using the first-order reaction model. The first-order reaction model is used to study the photocatalytic reaction kinetic parameters in the photocatalytic stage. The relationship between -Ln(C/C_0) and t was linearly fitted, and the apparent reaction rate constant k_{app} of the material was determined by slope.

4. Conclusions

In summary, g-C_3N_4-TiO_2/RCP composites were prepared by a mechanochemical method. The rough and porous structure of RCP not only provides a large number of loading sites, but also effectively slows down the agglomeration effect of g-C_3N_4-TiO_2. The uniform combination of g-C_3N_4-TiO_2 and RCP is achieved by physical adsorption and chemical bonding. The photocatalytic efficiency of pure g-C_3N_4-TiO_2 was improved after being combined with a certain amount of RCP. The improvement of photocatalytic performance of g-C_3N_4-TiO_2 by RCP is mainly achieved by better inhibition of hole–electron recombination. In addition, the application of g-C_3N_4-TiO_2/RCP composites on the surface of cement-based materials has achieved good results. The use of potassium silicate solution as a binder can firmly attach g-C_3N_4-TiO_2/RCP composites to the surface of cement-based materials. It not only improves the utilization of visible light in natural light by photocatalytic cement-based materials, but also realizes the reduction of photocatalysts. The concrete solid waste recycled RCP as the carrier of g-C_3N_4-TiO_2 has also been upgraded. The preparation of g-C_3N_4-TiO_2/RCP cement-based materials provides a promising route for the 'sustainable development' of photocatalytic cement-based materials.

Author Contributions: T.Y.: Writing–original draft, Investigation, Conceptualization. W.Y.: Resources, Supervision, Funding acquisition. All authors have read and agreed to the published version of the manuscript.

Funding: This work was supported by the National Key Research and Development Program of China (grant no. 2019YFC1906203).

Institutional Review Board Statement: Not applicable.

Informed Consent Statement: Not applicable.

Data Availability Statement: Not applicable.

Conflicts of Interest: The authors declare no conflict of interest.

References

1. Abou Saoud, W.; Assadi, A.A.; Guiza, M.; Bouzaza, A.; Aboussaoud, W.; Soutrel, I.; Ouederni, A.; Wolbert, D.; Rtimi, S. Abatement of ammonia and butyraldehyde under non-thermal plasma and photocatalysis: Oxidation processes for the removal of mixture pollutants at pilot scale. *Chem. Eng. J.* **2018**, *344*, 165–172. [CrossRef]
2. Ouachtak, H.; Akhouairi, S.; Haounati, R.; Addi, A.A.; Jada, A.; Taha, M.L.; Douch, J. 3,4-Dihydroxybenzoic acid removal from water by goethite modified natural sand column fixed-bed: Experimental study and mathematical modeling. *Desalination Water Treat.* **2020**, *194*, 439–449. [CrossRef]
3. Bengotni, L.; Trari, B.; Lebeau, B.; Michelin, L.; Josien, L.; Bengueddach, A.; Hamacha, R. Effect of diatomite addition on crystalline phase formation of TiO_2 and photocatalytic degradation of MDMA. *New J. Chem.* **2021**, *45*, 13463–13474. [CrossRef]
4. Diamanti, M.V.; Luongo, N.; Massari, S.; Spagnolo, S.L.; Daniotti, B.; Pedeferri, M.P. Durability of self-cleaning cement-based materials. *Constr. Build. Mater.* **2021**, *280*, 122442. [CrossRef]
5. Wang, F.Z.; Yang, L.; Sun, G.X.; Guan, L.Y.; Hu, S.G. The hierarchical porous structure of substrate enhanced photocatalytic activity of TiO_2/cementitious materials. *Constr. Build. Mater.* **2014**, *64*, 488–495. [CrossRef]
6. Yousefi, A.; Allahverdi, A.; Hejazi, P. Effective dispersion of nano-TiO_2 powder for enhancement of photocatalytic properties in cement mixes. *Constr. Build. Mater.* **2013**, *41*, 224–230. [CrossRef]
7. Adachi, T.; Latthe, S.S.; Gosavi, S.W.; Roy, N.; Suzuki, N.; Ikari, H.; Kato, K.; Katsumata, K.; Nakata, K.; Furudate, M.; et al. Photocatalytic, superhydrophilic, self-cleaning TiO_2 coating on cheap, light-weight, flexible polycarbonate substrates. *Appl. Surf. Sci.* **2018**, *458*, 917–923. [CrossRef]
8. Wang, X.; Wang, X.; Zhao, J.; Song, J.; Wang, J.; Ma, R.; Ma, J. Solar light-driven photocatalytic destruction of cyanobacteria by F-Ce-TiO_2/expanded perlite floating composites. *Chem. Eng. J.* **2017**, *320*, 253–263. [CrossRef]
9. Nomura, Y.; Fukahori, S.; Fujiwara, T. Thermodynamics of removing crotamiton and its transformation byproducts from water by a rotating advanced oxidation contactor with zeolite/TiO_2 composite sheets. *Chem. Eng. J.* **2020**, *380*, 122479. [CrossRef]
10. Padmanabhan, S.K.; Pal, S.; Haq, E.U.; Licciulli, A. Nanocrystalline TiO_2-diatomite composite catalysts: Effect of crystallization on the photocatalytic degradation of rhodamine B. *Appl. Catal. A-Gen.* **2014**, *485*, 157–162. [CrossRef]
11. Wang, B.; Zhang, G.X.; Sun, Z.M.; Zheng, S.L. Synthesis of natural porous minerals supported TiO_2 nanoparticles and their photocatalytic performance towards Rhodamine B degradation. *Powder Technol.* **2014**, *262*, 1–8. [CrossRef]
12. Feng, S.; Li, F. Photocatalytic dyes degradation on suspended and cement paste immobilized TiO_2/g-C_3N_4 under simulated solar light. *J. Environ. Chem. Eng.* **2021**, *9*, 105488. [CrossRef]
13. Gahlot, S.; Dappozze, F.; Mishra, S.; Guillard, C. High surface area g-C_3N_4 and g-C_3N_4-TiO_2 photocatalytic activity under UV and Visible light: Impact of individual component. *J. Environ. Chem. Eng.* **2021**, *9*, 105587. [CrossRef]
14. Zhong, W.; Wang, D.; Jiang, C.; Lu, X.; Zhang, L.; Cheng, X. Study on Visible Light Catalysis of Graphite Carbon Nitride-Silica Composite Material and Its Surface Treatment of Cement. *Crystals* **2020**, *10*, 490. [CrossRef]
15. Tian, Y.; Zhang, J.; Wang, W.; Liu, J.; Zheng, X.; Li, J.; Guan, X. Facile assembly and excellent elimination behavior of porous BiOBr-g-C_3N_4 heterojunctions for organic pollutants. *Environ. Res.* **2022**, *209*, 112889. [CrossRef] [PubMed]
16. Sun, S.J.; Li, C.Q.; Sun, Z.M.; Wang, J.; Wang, X.; Ding, H. In-situ design of efficient hydroxylated SiO_2/g-C_3N_4 composite photocatalyst: Synergistic effect of compounding and surface hydroxylation. *Chem. Eng. J.* **2021**, *416*, 129107. [CrossRef]
17. Jiang, X.-H.; Xing, Q.-J.; Luo, X.-B.; Li, F.; Zou, J.-P.; Liu, S.-S.; Li, X.; Wang, X.-K. Simultaneous photoreduction of Uranium(VI) and photooxidation of Arsenic(III) in aqueous solution over g-C_3N_4/TiO_2 heterostructured catalysts under simulated sunlight irradiation. *Appl. Catal. B Environ.* **2018**, *228*, 29–38. [CrossRef]
18. Hao, R.; Wang, G.; Tang, H.; Sun, L.; Xu, C.; Han, D. Template-free preparation of macro/mesoporous g-C_3N_4/TiO_2 heterojunction photocatalysts with enhanced visible light photocatalytic activity. *Appl. Catal. B Environ.* **2016**, *187*, 47–58. [CrossRef]
19. Ni, S.; Fu, Z.; Li, L.; Ma, M.; Liu, Y. Step-scheme heterojunction g-C_3N_4/TiO_2 for efficient photocatalytic degradation of tetracycline hydrochloride under UV light. *Colloids Surf. A Physicochem. Eng. Asp.* **2022**, *649*, 129475. [CrossRef]
20. Jia, J.; Wang, Y.; Xu, M.; Qi, M.-L.; Wu, Y.; Zhao, G. MOF-derived the direct Z-scheme g-C_3N_4/TiO_2 with enhanced visible photocatalytic activity. *J. Sol-Gel Sci. Technol.* **2019**, *93*, 123–130. [CrossRef]

21. Koci, K.; Reli, M.; Troppova, I.; Šihor, M.; Kupková, J.; Kustrowski, P.; Praus, P. Photocatalytic decomposition of N_2O over TiO_2/g-C_3N_4 photocatalysts heterojunction. *Appl. Surf. Sci.* **2017**, *396 Pt 2*, 1685–1695. [CrossRef]
22. Shen, G.; Pu, Y.; Cui, Y.; Jing, P. Easy synthesis of TiO_2/g-C_3N_4 Heterostructure Photocatalyst with Large Surface Area and Excellent Photocatalytic Activity. *Ceram. Int.* **2017**, *43*, S664–S670. [CrossRef]
23. Guesh, K.; Marquez-Alvarez, C.; Chebude, Y.; Diaz, I. Enhanced photocatalytic activity of supported TiO_2 by selective surface modification of zeolite Y. *Appl. Surf. Sci.* **2016**, *378*, 473–478. [CrossRef]
24. Li, C.Q.; Sun, Z.M.; Dong, X.B.; Zheng, S.L.; Dionysiou, D.D. Acetic acid functionalized TiO_2/kaolinite composite photocatalysts with enhanced photocatalytic performance through regulating interfacial charge transfer. *J. Catal.* **2018**, *367*, 126–138. [CrossRef]
25. Liao, G.; He, W.; He, Y.M. Investigation of Microstructure and Photocatalytic Performance of a Modified Zeolite Supported Nanocrystal TiO_2 Composite. *Catalysts* **2019**, *9*, 502. [CrossRef]
26. Akhtar, A.; Sarmah, A.K. Construction and demolition waste generation and properties of recycled aggregate concrete: A global perspective. *J. Clean. Prod.* **2018**, *186*, 262–281. [CrossRef]
27. Evangelista, L.; de Brito, J. Concrete with fine recycled aggregates: A review. *Eur. J. Environ. Civ. Eng.* **2014**, *18*, 129–172. [CrossRef]
28. Kim, J.; Grabiec, A.M.; Ubysz, A. An Experimental Study on Structural Concrete Containing Recycled Aggregates and Powder from Construction and Demolition Waste. *Materials* **2022**, *15*, 2458. [CrossRef]
29. Koshiro, Y.; Ichise, K. Application of entire concrete waste reuse model to produce recycled aggregate class H. *Constr. Build. Mater.* **2014**, *67*, 308–314. [CrossRef]
30. Kwon, E.; Ahn, J.; Cho, B.; Park, D. A study on development of recycled cement made from waste cementitious powder. *Constr. Build. Mater.* **2015**, *83*, 174–180. [CrossRef]
31. Oksri-Nelfia, L.; Mahieux, P.Y.; Amiri, O.; Turcry, P.; Lux, J. Reuse of recycled crushed concrete fines as mineral addition in cementitious materials. *Mater. Struct.* **2016**, *49*, 3239–3251. [CrossRef]
32. Wang, B.; Zhang, G.X.; Leng, X.; Sun, Z.M.; Zheng, S.L. Characterization and improved solar light activity of vanadium doped TiO_2/diatomite hybrid catalysts. *J. Hazard. Mater.* **2015**, *285*, 212–220. [CrossRef] [PubMed]
33. Haounati, R.; Alakhras, F.; Ouachtak, H.; Saleh, T.A.; Al-Mazaideh, G.; Alhajri, E.; Jada, A.; Hafid, N.; Addi, A.A. Synthesized of Zeolite@Ag_2O Nanocomposite as Superb Stability Photocatalysis Toward Hazardous Rhodamine B Dye from Water. *Arab. J. Sci. Eng.* **2023**, *48*, 169–179. [CrossRef]
34. Liao, G.; Yao, W. Upcycling of waste concrete powder into a functionalized host for nano-TiO_2 photocatalyst: Binding mechanism and enhanced photocatalytic efficiency. *J. Clean. Prod.* **2022**, *366*, 132918. [CrossRef]
35. Tang, Q.; Ma, Z.M.; Wu, H.X.; Wang, W. The utilization of eco-friendly recycled powder from concrete and brick waste in new concrete: A critical review. *Cem. Concr. Compos.* **2020**, *114*, 103807.
36. Geng, Z.; Xin, M.Y.; Zhu, X.T.; Xu, H.Y.; Cheng, X.; Wang, D. A new method for preparing photocatalytic cement-based materials and the investigation on properties and mechanism. *J. Build. Eng.* **2021**, *35*, 102080. [CrossRef]
37. Zhao, Y.; Wang, J.; Li, J.; Wang, M. Research progress on superhydrophobic coating on cement-based material. *New Chem. Mater.* **2022**, *50*, 219–224.
38. Zhang, X.; Li, H.; Harvey, J.T.; Liang, X.; Xie, N.; Jia, M. Purification effect on runoff pollution of porous concrete with nano-TiO_2 photocatalytic coating. *Transp. Res. Part D Transp. Environ.* **2021**, *101*, 103101. [CrossRef]
39. Manivannan, R.; Ryu, J.; Son, Y.-A. Controlled ultrasonic synthesis of TiO_2@C_3N_4 nanocomposites with porphyrin as a solid-state electron mediator: A promising material for pollutant discoloration under visible light. *Ceram. Int.* **2021**, *47*, 14399–14407. [CrossRef]
40. Lu, D.; Zhang, G.; Wan, Z. Visible-light-driven g-C_3N_4/Ti^{3+}-TiO_2 photocatalyst co-exposed {001} and {101} facets and its enhanced photocatalytic activities for organic pollutant degradation and Cr(VI) reduction. *Appl. Surf. Sci.* **2015**, *358*, 223–230. [CrossRef]
41. Wang, J.; Sun, S.J.; Ding, H.; Chen, W.T.; Liang, Y. Preparation of a composite photocatalyst with enhanced photocatalytic activity: Smaller TiO_2 carried on SiO_2 microsphere. *Appl. Surf. Sci.* **2019**, *493*, 146–156. [CrossRef]
42. Wang, J.; Sun, S.J.; Pan, L.; Xu, Z.Q.; Ding, H.; Li, W. Preparation and Properties of $CaCO_3$-Supported Nano-TiO_2 Composite with Improved Photocatalytic Performance. *Materials* **2019**, *12*, 3369. [CrossRef] [PubMed]
43. Liao, G.; Yao, W. Facile synthesis of porous isotype heterojunction g-C_3N_4 for enhanced photocatalytic degradation of RhB under visible light. *Diam. Relat. Mater.* **2022**, *128*, 109227. [CrossRef]
44. Tauc, J.; Grigorovici, R.; Vancu, A. Optical properties and electronic structure of amorphous germanium. *Phys. Status Solidi B* **1966**, *15*, 627–637. [CrossRef]